Inorganic Chemistry

Article

pubs.acs.org/IC

Excess Heat Capacity in Liquid Binary Alkali-Fluoride Mixtures

M. Beilmann,[†,‡] O. Beneš,*[,†] E. Capelli,[†] V. Reuscher,[†] R. J. M. Konings,[†] and Th. Fanghänel[†,‡]

[†]Institute for Transuranium Elements, European Commission, Joint Research Centre, P.O. Box 2340, 76125 Karlsruhe, Germany

[‡]Institute for Physical Chemistry, Ruprecht-Karls-University Heidelberg, Im Neuenheimer Feld 253, 69120 Heidelberg, Germany

ABSTRACT: Using drop calorimetry, we measured enthalpy increments of the LiF−KF, LiF−RbF, and LiF−CsF binary systems at temperatures above the melting point. Ten samples with different compositions (four compositions for LiF−KF, one composition for LiF−RbF, and five compositions for LiF−CsF) were prepared and measured between 884 K and 1382 K. To protect the calorimeter from corrosive fluoride vapor at high temperature, an encapsulating technique developed for this purpose was used. The samples were filled in nickel containers that were sealed by laser welding and afterward used for the measurements. From the obtained results, we derived the molar heat capacity functions of the respective samples. The heat capacities of the samples, having different compositions of the same binary system, were compared with the values for ideal behavior and the excess heat capacity function was determined for the entire composition range of the liquid solution. It was found that the excess heat capacities clearly depend on the cation radius and increase in the following order: LiF−NaF < LiF−KF < LiF−RbF < LiF−CsF.

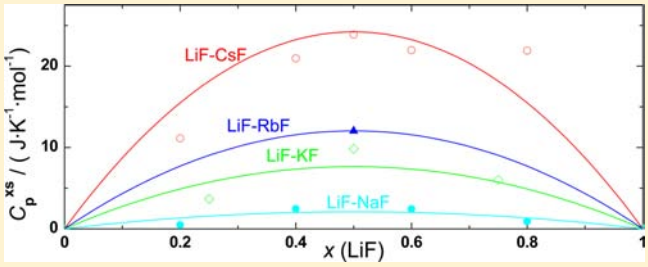

INTRODUCTION

Fluoride salts are considered as efficient energy storage and energy transfer materials in various fields ranging from nuclear[1] to solar energy production.[2] Pure fluoride salts, mostly alkali and alkaline-earth fluorides, are under investigation, which have advantageous properties for these applications, since they possess a high thermodynamic stability up to high temperatures (no dissociation) and low vapor pressures. This enhances the safety features of the system. In addition, the thermodynamic stability allows the process to reach high temperatures, which is required, e.g., for hydrogen production.[3]

By composing a mixture of these salts, some characteristics can be influenced very well. For example, the lowest melting point of a mixture can be several hundred degrees lower than those of the pure components. The density, viscosity, and heat capacity also are affected, and these characteristics have a big impact on the technical design of the system, affecting features such as the flow rate of the salt or the pumping power.

Information about the molar heat capacity of liquid fluoride salt mixtures is essential, since it determines the amount of energy that can be stored until the salt system reaches its maximum temperature. A high heat capacity has the advantage that more energy can be stored or transported and thus, the amount of salt can be reduced. Furthermore, the system will not be very sensitive to energy fluctuations, providing additional time to react in case of irregularities.

Therefore, in this work, we investigate the heat capacity of liquid mixtures of KF, RbF, and CsF with LiF. The results were compared with those of the LiF−NaF mixture, which were previously published by Beneš et al.;[4] this information allows us to establish a clear tendency that the heat capacity increases with increasing differences of the cation radii of the salt present in the melt.

RESULTS

In our drop calorimetry measurements, the sample consists of the salt encapsulated in a nickel capsule as described in the section of this paper entitled "Encapsulating Technique". For this reason, the area of the measured sample peak must be corrected for the contribution of the nickel. Therefore, enthalpy increment measurement of empty nickel capsules were done in a temperature range from 573 K to 1473 K. The obtained data proved that, for the used capsules, the thermodynamic data of nickel can be taken from Desai,[5] who evaluated enthalpy increment data from the available literature. The relative high mass of the nickel containers, 240 mg on average, compared to 70−120 mg of the salt, has a big influence on the area of the peak, which is between 30% and 60%, also depending on the salt examined. The nickel contribution was subtracted from the total value without uncertainty assigned to it. Hence, the average enthalpy values of the salt have a relative large uncertainty, which is the standard deviation of the enthalpy values at the given temperature. For this reason, several drops were done at the same temperature to reduce the uncertainty. Tables 1 and 2 list the average enthalpy increment values $(H^{T_m} - H^{298\ K})$ with the number of drops n for the different measurements. H^{T_m} denotes the enthalpy of the sample at the measured temperature.

The enthalpy measurements are repeated at several temperatures, and the average enthalpy values for each temperature are plotted versus the measured temperatures for the particular composition. An example is shown in Figure 1. Here, the uncertainty of the enthalpies are obtained by calculating the standard deviation of the measured data at the same temperature. According to

Received: October 4, 2012
Published: February 19, 2013

   dx.doi.org/10.1021/ic302168g | Inorg. Chem. 2013, 52, 2404−2411

Table 1. Enthalpy Increment Measurements of the $(Li_xK_{1-x})F_x$ and the $(Li_xRb_{1-x})F_x$ Liquid Solutions Done in This Study

T (K)	$H^{T_m} - H^{298\ K}$ (J mol^{-1})	n	T (K)	$H^{T_m} - H^{298\ K}$ (J mol^{-1})	n
		LiF−KF			
	KF			$(Li_{0.75}K_{0.25})F$	
1157.7	82910 ± 4837	11	1157.9	72763 ± 4584	18
1169.5	86563 ± 3531	12	1169.9	72833 ± 4943	12
1182.3	87364 ± 8244	9	1182.8	73745 ± 2346	6
1194.1	82753 ± 6976	11	1194.8	76633 ± 3282	10
1206.9	82220 ± 11784	4	1207.9	76905 ± 6014	6
1218.9	88484 ± 5564	6	1219.6	75278 ± 4787	12
1231.2	90518 ± 4209	4	1232.7	78016 ± 3892	6
1243.4	87403 ± 6362	6	1244.7	79538 ± 5547	6
1255.9	88381 ± 5036	10	1257.4	79755 ± 5537	6
1268.2	91451 ± 3667	6	1269.6	81590 ± 5066	6
1280.6	96758 ± 2441	4	1282.5	81400 ± 2533	11
1292.3	96967 ± 3980	5	1294.5	84262 ± 4069	6
1305.1	96928 ± 8169	10	1307.2	81601 ± 3909	6
1317.2	93513 ± 4590	6	1319.4	83158 ± 4865	8
1329.8	96673 ± 9002	10	1332.4	84287 ± 4769	12
1341.6	94327 ± 3656	6	1344.2	84922 ± 5110	12
	$(Li_{0.50}K_{0.50})F$			$(Li_{0.25}K_{0.75})F$	
884.5	55401 ± 1756	10	1157.5	78052 ± 3072	12
909.2	60204 ± 3273	8	1182.0	79374 ± 4301	16
934.1	61231 ± 3257	8	1206.8	80953 ± 3128	8
959.0	62609 ± 4320	8	1231.2	83734 ± 5048	16
983.9	64637 ± 4439	10	1256.0	83830 ± 3294	8
1008.8	63935 ± 3771	12	1280.5	87751 ± 2553	8
1033.6	70087 ± 6003	6	1305.1	89687 ± 4174	12
1058.5	70370 ± 4354	8	1329.6	89850 ± 3501	12
1083.2	71023 ± 2463	10			
	$(Li_{0.50}Rb_{0.50})F$				
985.6	64006 ± 2076	6			
1010.6	65982 ± 2362	6			
1035.6	68688 ± 4357	9			
1060.6	67597 ± 3015	6			
1085.6	69863 ± 3851	3			
1110.6	73264 ± 3953	3			
1135.5	76116 ± 3156	6			
1160.7	76333 ± 1286	3			
1185.7	78961 ± 2392	6			
1210.7	80407 ± 3260	6			
1235.7	84506 ± 2295	3			
1260.8	85500 ± 4956	3			
1286.0	88804 ± 3353	3			

eq 1, the heat capacity of the sample $C_p(T)$ can be determined as the derivative of the enthalpy increment, with respect to temperature.

$$C_p(T) = \frac{dH}{dT} \quad (1)$$

All measured compositions indicated a linear behavior of the enthalpy increments, with respect to temperature. Hence, the data were fitted using a weighted least-squares linear fit. To every data point, the factor $w_i = 1/\sigma_i^2$ was assigned as weight, where σ_i is the size of the error bar of data point i.

Once the heat capacities of the different compositions of a particular system are determined, the excess heat capacities are obtained by subtracting the values calculated according to the

Table 2. Enthalpy Increment Measurements of the $(Li_xCs_{1-x})F_x$ Liquid Solution Done in This Study

T (K)	$H^{T_m} - H^{298\ K}$ (J mol^{-1})	n	T (K)	$H^{T_m} - H^{298\ K}$ (J mol^{-1})	n
		LiF−CsF			
	$(Li_{0.20}Cs_{0.80})F$			$(Li_{0.40}Cs_{0.60})F$	
984.1	66205 ± 8138	12	884.8	58228 ± 4686	4
1009.0	72499 ± 6094	12	909.6	61983 ± 4818	3
1034.0	69199 ± 4192	6	934.5	59030 ± 2963	4
1058.8	71637 ± 6035	12	959.3	65318 ± 5018	4
1083.5	75098 ± 5806	6	984.2	68132 ± 3577	8
1108.6	80350 ± 3196	6	1009.1	67254 ± 5423	4
1133.2	79924 ± 1834	6	1034.0	66951 ± 3952	4
1158.4	80687 ± 4100	6	1058.4	75751 ± 8126	7
1183.0	84513 ± 4064	6	1083.7	74524 ± 4552	4
1208.2	85871 ± 4814	6	1108.5	74010 ± 3654	4
1232.7	90543 ± 3861	6	1133.0	80189 ± 1904	9
	$(Li_{0.50}Cs_{0.50})F$			$(Li_{0.60}Cs_{0.40})F$	
935.2	57647 ± 4374	5	934.2	58681 ± 5187	4
960.0	62907 ± 4530	10	959.3	66507 ± 2822	4
984.8	62563 ± 3332	4	984.1	67983 ± 2638	4
1009.4	64648 ± 2019	5	1009.0	68338 ± 4239	4
1034.1	67641 ± 3368	5	1034.0	68626 ± 1790	4
1058.8	67578 ± 3040	10	1058.7	75827 ± 6287	4
1083.4	73279 ± 4047	8	1083.6	70338 ± 6850	8
1108.2	73114 ± 5413	10	1108.4	78095 ± 4950	7
1132.8	75637 ± 4453	9	1133.3	82258 ± 9505	8
1157.5	78079 ± 2848	5	1158.1	87950 ± 6439	4
1182.0	83616 ± 5842	10			
	$(Li_{0.80}Cs_{0.20})F$				
1083.7	74503 ± 5787	4			
1133.9	81012 ± 2170	4			
1182.9	78646 ± 2660	4			
1108.2	73677 ± 3411	3			
1158.1	78247 ± 3546	4			
1207.7	84118 ± 4918	4			
1058.6	71666 ± 5234	4			
1232.5	86680 ± 3418	4			
1257.4	86219 ± 2584	4			
1282.6	90798 ± 2710	4			

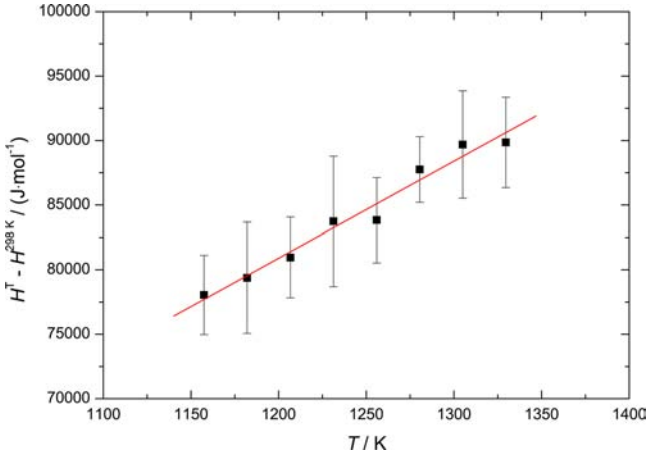

Figure 1. Example of the enthalpy increment results of the $Li_{0.25}K_{0.75}F$ composition. The straight line is a weighted least-squares linear fit of the data, giving C_p = (75.0 ± 5.5) J mol^{-1} K^{-1}.

Neumann−Kopp rule, representing ideal behavior. To calculate the ideal values of a mixture, the heat capacities of the pure

dx.doi.org/10.1021/ic302168g | Inorg. Chem. 2013, 52, 2404−2411

compounds are weighted by their mole fractions, according to $C_p(A_xB_{1-x}) = xC_p(A) + (1-x)C_p(B)$, where A and B represent the pure compounds LiF, NaF, KF, RbF, and CsF, respectively, and x denotes the mole fraction. The excess heat capacities are plotted afterward, versus the composition, and fitted mathematically, using a one-parameter function for a regular solution. The formula is shown in eq 2, where A is the parameter to be determined.

$$y = Ax(1-x) \quad (2)$$

LiF−KF System. To determine the heat capacity function of the $(Li_xK_{1-x})F_x$ melt, enthalpy increments of KF and three different compositions (x = 0.25, 0.50, and 0.75) were measured in the temperature range from 1158 K to 1344 K and from 884 K to 1083 K for the composition $Li_{0.50}K_{0.50}F$. As an example, Figure 1 shows the average values of the enthalpy increments of $Li_{0.25}K_{0.75}F$ versus the temperature with the weighted least-squares linear fit (red solid line). The plot of the heat capacity values for the entire system is shown in Figure 2, where the straight

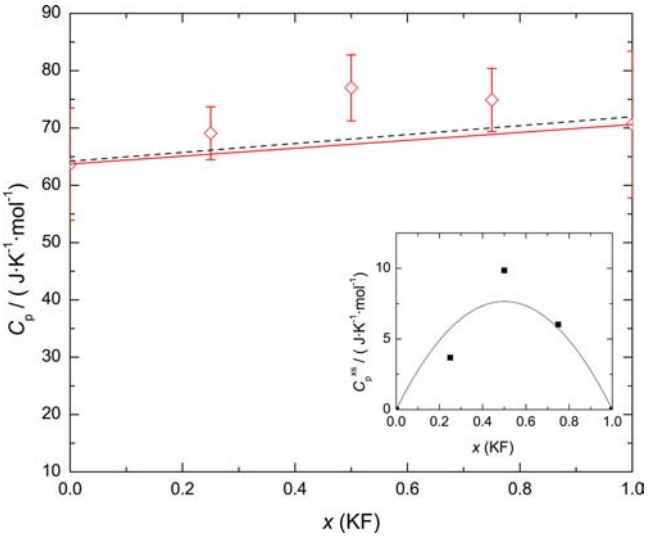

Figure 2. (◇) Heat capacity of the $(Li_xK_{1-x})F_x$ liquid solution measured in this study. The solid line indicates an ideal behavior based on the heat capacity of KF, which was measured in this work, and the heat capacity of LiF, which has been taken from ref 4. The dashed line represents an ideal behavior considering the data from the literature.[6] In the inset graph, the excess heat capacity of the $(Li_xK_{1-x})F_x$ liquid solution is plotted versus the composition; the solid line represents the fit according to eq 3.

line indicates the values calculated by the Neumann−Kopp rule. Here, the solid line considers the values of the end-members measured in this study and the dashed line is related to the literature values. Both results agree very well.

The molar heat capacities of the intermediate compositions are found to be higher than the Neumann−Kopp value, indicating an excess heat capacity of the $(Li_xK_{1-x})F_x$ melt. The insert graph in Figure 2 shows the difference between the measured heat capacities and the ideal values (Neumann−Kopp), which were calculated considering the heat-capacity values of the end-members measured in this study for KF and in our previous study for LiF.[4] Equation 3 describes the excess heat-capacity function of the system, obtained by fitting eq 2 to the data.

$$C_p^{xs}\ (\mathrm{J\ mol^{-1}\ K^{-1}}) = x_{LiF}x_{KF}(30.6 \pm 4.3) \quad (3)$$

Tables 1 and 3 specify the data of the enthalpy increments and the molar heat capacities of the different compositions, respectively.

Table 3. Heat Capacities of Various Compositions Measured in This Work

composition	C_p (J mol^{-1} K^{-1})	temperature range (K)
KF	70.6 ± 12.8	1158−1342
$(Li_{0.75}K_{0.25})F$	69.1 ± 4.6	1158−1344
$(Li_{0.50}K_{0.50})F$	77.1 ± 5.8	884−1083
$(Li_{0.25}K_{0.75})F$	75.0 ± 5.5	1157−1330
$(Li_{0.50}Rb_{0.50})F$	79.4 ± 3.4	985−1286
$(Li_{0.20}Cs_{0.80})F$	91.1 ± 8.2	984−1233
$(Li_{0.40}Cs_{0.60})F$	89.8 ± 7.7	884−1133
$(Li_{0.50}Cs_{0.50})F$	91.0 ± 5.5	935−1182
$(Li_{0.60}Cs_{0.40})F$	87.4 ± 16.9	934−1158
$(Li_{0.80}Cs_{0.20})F$	76.2 ± 11.6	1059−1283

LiF−CsF System. The enthalpy increments of samples with five different $(Li_xCs_{1-x})F_x$ compositions (x = 0.20, 0.40, 0.50, 0.60, and 0.80) have been measured at temperatures higher than the melting temperature of the respective samples, in order to determine their high-temperature heat-capacity function. Together with the measurements of LiF, which were taken from ref 4, and the measurements of pure CsF, published in a recent study,[7] the measured samples covered the full composition range of the binary LiF−CsF system. The heat capacities of the samples were obtained from the enthalpy increments using the same approach as that already explained in the Results section. Subtracting the ideal values, calculated with the Neumann−Kopp rule, from the measured values, the excess heat-capacity contributions were determined and are shown in the insert graph of Figure 3. By fitting eq 2 to the obtained results, the molar excess heat-capacity

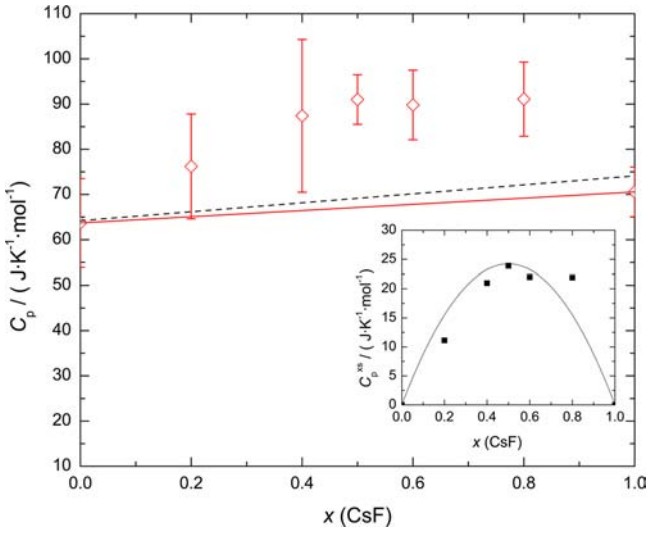

Figure 3. (◇) Heat capacity of the $(Li_xCs_{1-x})F_x$ liquid solution measured in this study. The solid line indicates an ideal behavior based on the heat capacity of CsF, which was measured in our previous work,[7] and the heat capacity of LiF, which has been taken from ref 4. The dashed line represents an ideal behavior, considering the data from the literature.[6] In the inset graph, the excess heat capacity of the $(Li_xCs_{1-x})F_x$ liquid solution is plotted versus the composition. The solid line represents the fit according to eq 4.

dx.doi.org/10.1021/ic302168g | Inorg. Chem. 2013, 52, 2404−2411

function of the $(Li_xCs_{1-x})F_x$ liquid solution was determined and is expressed by eq 4.

$$C_p^{xs}\ (J\ mol^{-1}\ K^{-1}) = x_{LiF}x_{CsF}(96.9 \pm 5.9) \quad (4)$$

The data of the enthalpy increments and the heat capacities are listed in Tables 2 and 3.

LiF−RbF System. The enthalpy increments of the $Li_{0.50}Rb_{0.50}F$ composition were measured in the temperature range from 986 K to 1286 K. The results of these measurements are shown in Table 1. Using the same formalism as that for the LiF−KF and LiF−CsF systems, the high-temperature heat capacity of the measured composition was derived from the obtained data. In order to calculate the excess heat capacity of the $Li_{0.50}Rb_{0.50}F$ mixture, the derived value was reduced by the heat-capacity value, implying an ideal behavior of the $(Li_xRb_{1-x})F_x$ liquid solution, which was calculated according to the Neumann−Kopp rule. Since the heat capacities of the alkali-fluoride salts LiF,[4] NaF,[4] KF, and CsF,[7] which were derived from the enthalpy increment measurements with the present equipment using the encapsulation approach, showed good agreement with literature values as indicated in Figures 2, 3, and 5 (shown later in this study); the literature value of RbF[6] was used in this study.

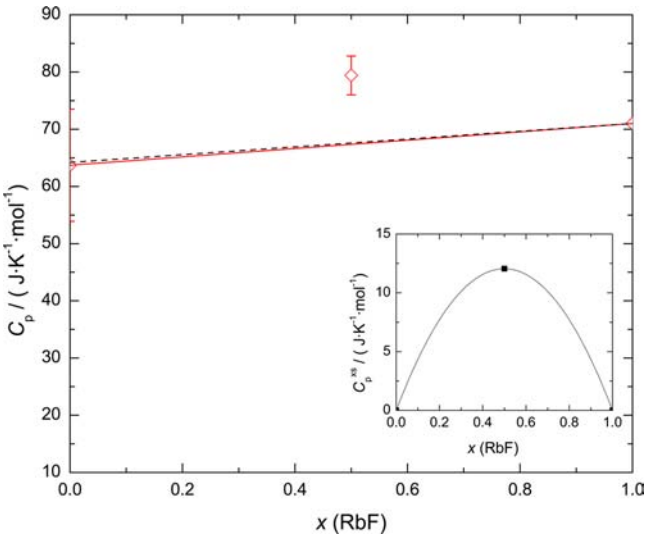

Figure 4. (◇) Heat capacity of the $(Li_xRb_{1-x})F_x$ liquid solution measured in this study. The solid line indicates an ideal behavior based on the heat capacity of RbF, which was taken from the literature,[6] and the heat capacity of LiF taken from ref 4. The dashed line represents an ideal behavior considering both data from the literature.[6] In the inset graph, the excess heat capacity of the $(Li_xRb_{1-x})F_x$ liquid solution is plotted versus the composition. The solid line represents the fit according to eq 5.

The inset graph in Figure 4 indicates the excess heat capacity of the $Li_{0.50}Rb_{0.50}F$ composition and the fit of eq 2 to this data point. It is evident that there was no uncertainty assigned to the fitted parameter A of this equation, since it is fitted to only one value at $x = (1 - x) = 0.5$. The investigation of the LiF−KF and LiF−CsF systems showed that the respective fit of eq 2 to the excess heat-capacity data agrees well with the data points at $x = 0.5$, as shown in the inset graphs in Figures 2 and 3. We took this result as verification that the applied procedure is also applicable to calculate the excess heat-capacity function of the $(Li_xRb_{1-x})F_x$ liquid solution based only on one value. To assess the uncertainty, we took the average value of the uncertainties, expressed as a percentage, of eqs 3, 4, and 6, which was calculated to be 5.8 J mol^{-1} K^{-1}. The total excess heat capacity is given by eq 5.

$$C_p^{xs}\ (J\ mol^{-1}\ K^{-1}) = x_{LiF}x_{RbF}(48.2 \pm 5.8) \quad (5)$$

LiF−NaF System. The data of the enthalpy increment measurements and heat capacity determination of the $(Li_xNa_{1-x})F_x$ liquid solution were already published in an earlier article[4] by our group and is used in this study without any changes. LiF, NaF, and four different compositions (x = 0.20, 0.40, 0.60, and 0.80) have been measured in the temperature range from 1230 K to 1470 K and from 1320 K to 1540 K for pure NaF, because of the higher melting point of this compound. From the heat capacity determination of the liquid solution, a slight deviation from the Neumann−Kopp rule was found, as can be seen in Figure 5. The excess heat-capacity function of the $(Li_xNa_{1-x})F_x$ liquid solution is given by eq 6.

$$C_p^{xs}\ (J\ mol^{-1}\ K^{-1}) = x_{LiF}x_{NaF}(8.3 \pm 1.3) \quad (6)$$

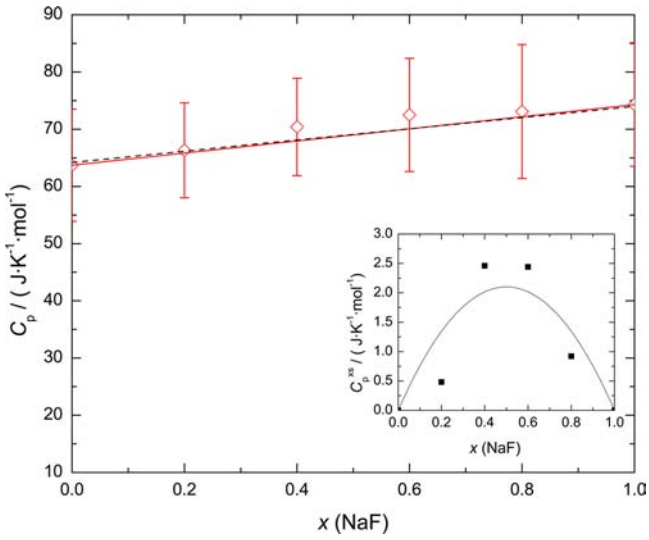

Figure 5. (◇) Heat capacity of the $(Li_xNa_{1-x})F_x$ liquid solution taken from ref 4. The solid line indicates an ideal behavior based on the measured heat capacities of LiF and NaF, using drop calorimetry. The dashed line represents an ideal behavior considering the data from the literature.[6] In the inset graph, the excess heat capacity of the $(Li_xNa_{1-x})F_x$ liquid solution is plotted versus the composition. The solid line represents the fit according to eq 6.

DISCUSSION AND CONCLUSIONS

Pure Alkali-Fluoride Salts. To be able to understand the results that we obtained in this study, it is necessary to have a closer look at the molecular structure of molten alkali-fluoride salts and salt mixtures, which was discussed in a recent review by Rollet et al.[8]

In salts, the inner arrangement of the ions is dominated by Coulomb attraction of unlike ions and repulsion of like ions. Even in the melt, where the ions have a relative high kinetic energy, this leads to a medium-range order structure in which a cation is surrounded by anions and vice versa.

Monte Carlo calculations by Baranyai et al.[9] showed that, in the pure alkali-fluoride salts, the first nearest-neighbor

dx.doi.org/10.1021/ic302168g | Inorg. Chem. 2013, 52, 2404−2411

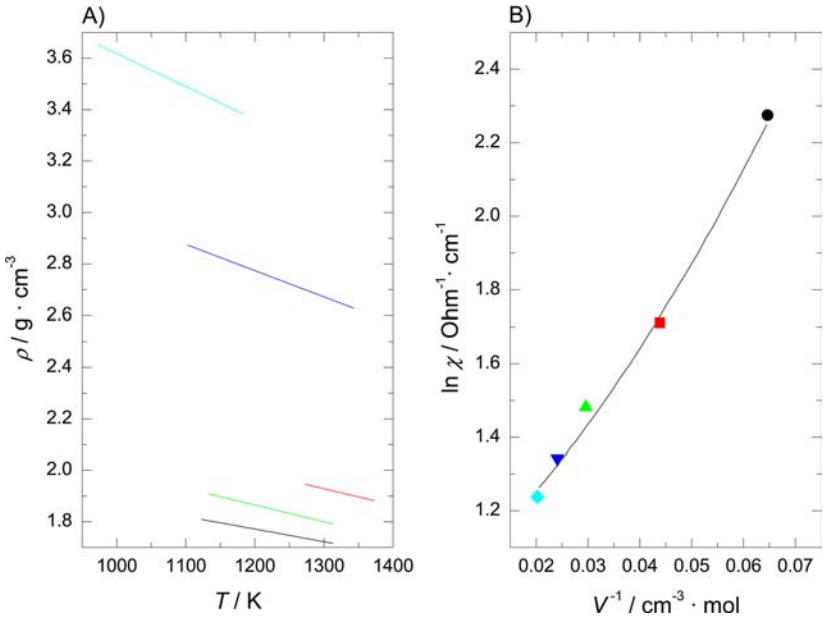

Figure 6. (A) Plot of the densities of molten alkali-fluoride salts.[15] [From top to bottom: CsF, RbF, NaF, KF, LiF.] (B) Plot of the logarithm of specific conductivity of molten salts versus the reciprocal molar volume at 1400 K. The data are read from Figure 1 in the Dedyukhin et al.[12] publication, using graphics analysis software. [Legend: (black circle, ●) LiF, (red square, ■) NaF, (green triangle, ▲) KF, (dark blue inverted triangle, ▼) RbF, (light blue diamond, ◆) CsF.]

coordination number increases from Li^+ to Cs^+. The reason for this is most probably the difference in the cation size, which also influences other properties, such as the polarizability. Because of the cation size, the binding force characteristics inside the melt are also changed. From Raman scattering measurements of LiF, KF, and CsF, Dracopoulos et al.[10] concluded that, in LiF, the F^- ions are almost in contact with each other, whereas the small Li^+ is kept in an anion shell. In this melt, the repulsive anion−anion interaction dominates the spectrum. Also, as the size of the cations increases, the distances between neighboring F ions increase and the dipole−induced-dipole interaction between cations and anions becomes more and more important while going from LiF to KF and CsF.

The character of the chemical bond between different cations and a common anion is also determined by the size and, thus, the polarizability of the cations. Because of the small radius of the Li^+ ion in LiF, the attractive interaction between the atomic core and the electrons is very strong and the high charge density distorts the electronic cloud around F^-, leading to a slight covalent character of the bond in this ionic compound. On the other hand, the radius of the Cs^+ cation in CsF is so big that the outer electrons are only weakly influenced by the field of the atomic core. The two ions in CsF are more independent from each other with a higher ionic character of the chemical bond than in LiF. This is clearly shown in a study by Salanne et al.,[11] who evaluated the anion polarizabilities in the condensed phase of LiF, NaF, KF, and CsF. The ionic size of the F^- anion is increasing in parallel to the size of the cation and approaches the value of the free F^- anion in CsF. Another indication is evident from the fact that after francium, Cs has the lowest electronegativity on the Pauling scale (0.79), whereas F has the highest electronegativity value (4), leading to the most ionic chemical compound, CsF.

The size of the cations, having a common anion, also influences the macroscopic properties of the melt. A good example is the electrical conductivity, which is mainly determined by the ion mobility, and this is strongly related to the size of the ions. Dedyukhin et al.[12] compared the electrical conductivity of the alkali fluorides and showed a dependence on the molar volume of the salts.

This is evident from the decrease of the electrical conductivity with an increase of the cation and, thus, also the anion size, as shown in Figure 6. Together with data of the density of the molten salts, which is rising from LiF to CsF,[13] the behavior of the electrical conductivity can be interpreted with a lower mobility of large ions. The thermal conductivity (λ) follows the same trend. This is shown in the empirical formula of Khoklov et al.[14]

$$\lambda = -0.34 + 0.5 \times 10^{-3}T + \frac{32.0}{M} \quad (7)$$

where λ has units of W m^{-1} K^{-1}, M is the molecular mass of the salt (in g mol^{-1}), and T is the temperature (in Kelvin). Here, it is expected that next to ion diffusion in the melt, vibrations of short-range order structures have a high influence. Figure 6 summarizes the density and electrical conductivity of the alkali-fluoride melts.

Salt Mixtures. When mixing LiF with an alkali fluoride with a cation of bigger size in the liquid state, the original internal structure is disturbed and a reorganization of the melt takes place. Experimental data from Holm et al.[13] show that, for the LiF−NaF, LiF−KF, and LiF−RbF mixtures, the enthalpy of mixing becomes more negative with increasing size of the cation. Unfortunately, because of the high vapor pressure, the LiF−CsF system was investigated with a different experimental procedure. Here, solid LiF was mixed with liquid CsF, whereas the other mixtures were investigated using the liquid−liquid method. This complicates the comparison of the different salt systems; however, in total, the results of that study indicate a strong interaction of the cations, which increases with the difference of the cation radii. In a later publication, Macleod et al.[16] compared some of the results from Holm and Kleppa[13] with their own and other literature data and found significant differences in the values. These were attributed to difficulties arising from the direct-reaction technique used by Holm and Kleppa[13] at high temperatures. However, besides the

dx.doi.org/10.1021/ic302168g | Inorg. Chem. 2013, 52, 2404−2411

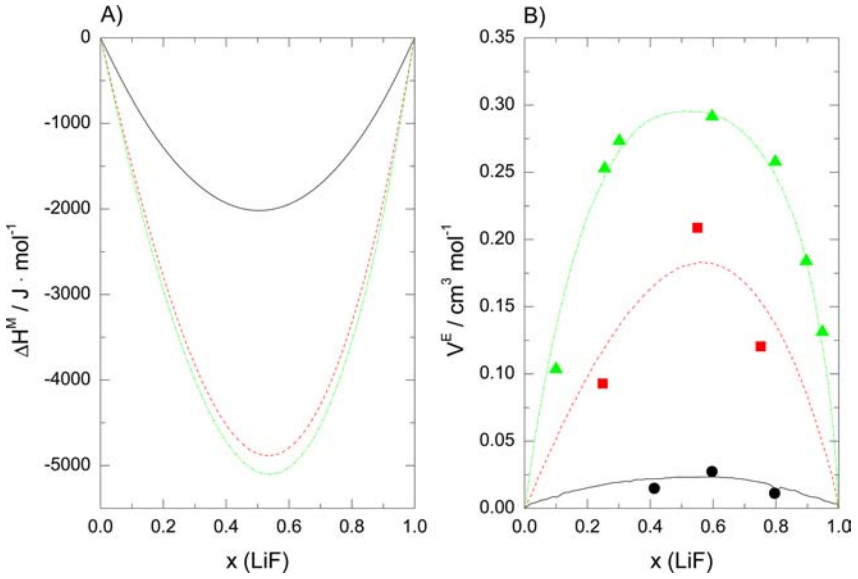

Figure 7. (A) Plot of the enthalpies of mixing versus the mole fraction of LiF (x(LiF)). [Legend: (solid black line, —) LiF−NaF, (red dashed line, - - -) LiF−KF, and (green dash-dotted line, - · - ·) LiF−RbF. The data are taken from ref 13.] (B) Plot of the excess molar volumes of mixing versus the mole fraction of LiF at 1173 K. [Legend: (solid black line, —) LiF−NaF, (red dashed line, - - -) LiF−KF, and (green dash-dotted line, - · - ·) LiF−RbF. Experimental data: (black circle, ●) LiF−NaF, (red square, ■) LiF−KF, (green triangle, ▲) LiF−RbF. The data are taken from Figure 1 in the publication by Holm,[18] using graphics analysis software.]

differences in the absolute values, the trend of the data was confirmed. Figure 7 shows the enthalpies of mixing between LiF and the other alkali fluorides, according to ref 13.

The influence of the interaction forces inside the melt can be seen in the LiF−KF system, where the mobility of Li^+ as well as K^+ decrease upon mixing. Using molecular dynamics (MD) calculations, Ribeiro[17] attributed this effect to an intermediate range order beyond the first-neighbor shell. In the LiCl−KCl system, it is known that the mobility of Li^+ decreases whereas the mobility of K^+ increases. For that system, the calculations show a strengthening of the small cation−anion bonds, followed by a weakening of the large cation−anion association. Thus, the small cation is immobilized and the large cation has a higher mobility. The calculations show similar effects also for the LiF−KF couple but there are some structural relaxation differences in a range beyond the first neighbors. A stronger intermediate range order is expected in the LiF−KF melt, which is most probably the cause for the different cation mobilities.

The theory that an intermediate range order develops in fluoride melts is supported by Raman measurements of Dracopoulos et al.[10] They investigated the LiF−KF and LiF−CsF systems and found next to a strengthening of the Li−F bonds (short-range overlap) long-lived species in both melts. These associations have a common structure of the type $(LiF_x)A$ (where A = K, Cs). Around a Li^+ cation, the first coordination shell is occupied by F^- ions, whereas, in the second coordination sphere, there are A^+ cations associated. The lifetimes of these species were estimated to be 0.3 ps for the LiF−KF system and 0.8 ps for the LiF−CsF system. This clearly demonstrates the higher thermodynamic stability of complexes formed in the system with a higher difference in the cation radii.

In this context, it is understandable that Holm and Kleppa[13] found a clear trend in the excess molar volumes of mixing. These volumes are increasing in alkali-fluoride mixtures in the following order: LiF−NaF < LiF−KF < LiF−RbF. An explanation could be the formation of complex species in the melt with stabilities according to the cation radii differences, which disturb the closely packed structure of the ions and cause the excess volume. The trend of the excess molar volumes of mixing is displayed in Figure 7.

The results that we obtained in this study fit very well in this context. For the heat capacity of a liquid, the main contribution of storing the energy usually arises from vibration mechanisms of short-range-ordered structures, if available. As described in the previous paragraphs, there are several strong indications that complex species are present in the melt of mixtures between lithium fluoride (LiF) and other alkali fluorides. With a higher stability and longer lifetime of these complexes, assuming a similar formation rate within the alkali-metal series, their concentration is higher and they can store more energy before collapsing. This explains the trend and the significant values we found in the excess heat capacity of alkali-fluoride mixtures. Figure 8 shows a superposition of the functions valid for the various systems with the respective excess heat-capacity data. From this graph, it is evident that the excess heat capacity of the liquid solution increases in the following order: LiF−NaF < LiF−KF < LiF−RbF < LiF−CsF.

Our results compare nicely with the heat-capacity measurements conducted at Oak Ridge National Laboratories. Values for one composition from each of the LiF−NaF, LiF−KF, and LiF−RbF systems are reported in ref 19. After conversion to the same units, they agree well with the values calculated with our fit, which is shown in detail in Table 4. Here, only the value for the $(Li_{0.60}Na_{0.40})F$ composition shows a bigger discrepancy.

To have a better overview of how sensitive the heat capacity is to the size mismatch of the cations, we plotted the A parameter of the regular solution fit of the investigated systems versus the difference between the A^+ cation radii (Na^+ = 95 pm, K^+ = 133 pm, Rb^+ = 152 pm, Cs^+ = 165 pm, all with octahedral coordination, taken from ref 20) and the Li^+ cation radius ($r(Li^+)$ = 60 pm). This value is necessarily found at a composition of $(Li_{0.50}A_{0.50})F$, because of the symmetry of the function used for the fit. The graph is shown in Figure 9, from which it is evident

dx.doi.org/10.1021/ic302168g | Inorg. Chem. 2013, 52, 2404−2411

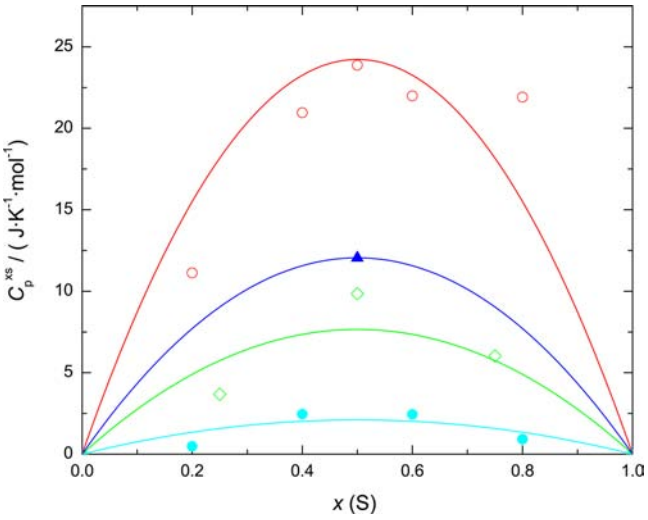

Figure 8. Superposition of the excess heat capacities with the respective regular solution fits. [Legend: (red open circles, ○) $(Li_xCs_{1-x})F_x$ liquid solution; (dark blue solid triangles, ▲) $(Li_xRb_{1-x})F_x$ liquid solution; (green open diamonds, ◇) $(Li_xK_{1-x})F_x$ liquid solution; and (light blue solid circles, ●) $(Li_xNa_{1-x})F_x$ liquid solution.]

Table 4. Comparison of Heat-Capacity Values of $Li_{0.60}Na_{0.40}F$, $Li_{0.50}K_{0.50}F$, and $Li_{0.43}Rb_{0.57}F$, Using Measurements Done in This Work and Measurements Conducted at Oak Ridge National Laboratories. The values were converted to the same units

	C_p (J mol^{-1} K^{-1})		
composition	this work	ref 19	ΔC_p (J mol^{-1} K^{-1})
$Li_{0.60}Na_{0.40}F$	69.4	78.53	1.3
$Li_{0.50}K_{0.50}F$	77.1	77.35	5.8
$Li_{0.43}Rb_{0.57}F$	79.7	84.01	3.4

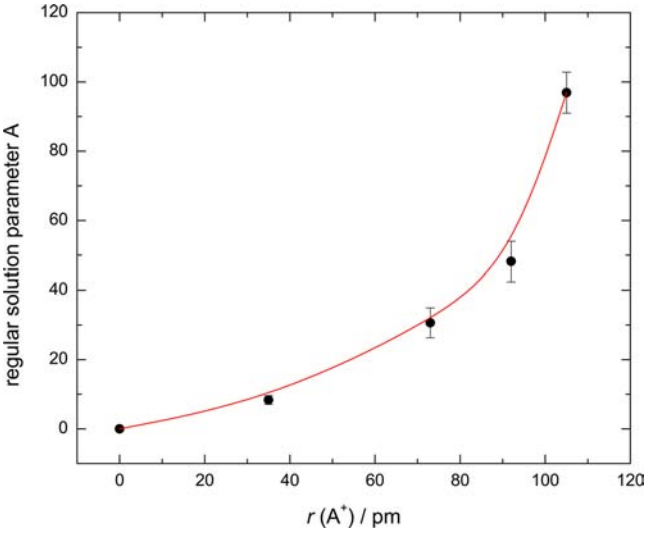

Figure 9. Plot of the *A* parameter of the regular solution fit (1:1 ratio of Li^+/A^+) versus the difference in cation radii in the melt. (A^+ = Li^+, Na^+, K^+, Rb^+, Cs^+; from left to right).

that the excess heat capacity (C_p^{xs}) is highly dependent on the size difference of the cations in the mixture.

It is very interesting to get an idea about the order of magnitude of the excess heat capacities. This can be illustrated by calculating the percentage of $C_p^{xs,max}$ from the total value ($C_p^{xs,max}$ plus ideal value at $(Li_{0.50}A_{0.50})F$, with A = Na, K, Rb, Cs, as per the Neumann−Kopp rule), using the following formalism:

$$\frac{C_p^{xs,max}}{(C_p^{xs,max} + C_p^{ideal})} \times 100 \quad (8)$$

These values range from only 3% for LiF−NaF (11% for LiF−KF and 18% LiF−RbF) to a considerable value of 39% for the LiF−CsF liquid solution; needless to say, these are the maximum values.

The clear trend of the excess heat capacity of alkali-fluoride mixtures is extremely important when considering fluoride salts for energy storage or energy transport systems and should be taken into account for the various designs. Similar studies considering also the effect of divalent, trivalent, and tetravalent fluoride salts can be very useful for the purpose of predicting the heat capacity of more-complex liquids.

EXPERIMENTAL SECTION

Encapsulating Technique. At high temperature, fluoride salts and their vapor are known to be corrosive to many materials. Although alkali fluorides are very stable compounds up to high temperatures and have usually only low to moderate vapor pressures (6.8×10^{-4} bar for LiF, 5.6×10^{-4} bar for NaF, 7.1×10^{-3} bar for KF, 2.1×10^{-2} bar for RbF, 1.2×10^{-1} bar for CsF; all at 1300 K), fluoride vapor can cause considerable damage to thin platinum/platinum−rhodium wires used for the thermocouples (S-type) in the calorimeter, which was used in this work. For high temperatures, see Table 3; for experiments with long duration (3−5 h), it was necessary to encapsulate the samples using a laser-welding-based encapsulation technique, as described in detail by Beneš et al.,[4] with slight modifications.

Compared to the described procedure,[4] the main difference is that, in this work, the capsules were welded under vacuum ($\sim 4 \times 10^{-4}$ bar) to generate less pressure inside the capsules at high temperatures. Especially without an argon atmosphere, it is necessary to prevent the nickel capsule—and, thus, the salt inside—from getting too hot during the welding process, since, at high temperatures, the overpressure caused by evaporation of the salt leads to leaking of the capsule. For this reason, the weld was performed in several steps, 4−6 s each step, rather than in one step. Another measure was to fill the nickel crucibles with salt pellets, instead of salt powder, as explained in the following Sample Preparation section, to reduce the contact area between the capsule and the salt.

Sample Preparation. The preparation of the salt samples was done in an argon glovebox with a water content of <50 ppm. The pure alkali-fluoride salts were purchased from Alfa Aesar with purities of 99.99% for LiF, 99.995% for NaF, 99.99% for KF, 99.9% for CsF, and 99.7% for RbF. Prior to the measurements and mixture preparation, the pure salts were heated at 623 K for 3 h under argon/hydrogen (3%) atmosphere to remove traces of possibly absorbed moisture. Here, the H_2 content in the protective gas prevents oxidation of the salt. The melting temperatures of the dried compounds were measured using differential scanning calorimetry (DSC) under the same conditions described in an earlier publication,[21] and the obtained temperatures were compared to literature data. The melting temperatures of the used fluoride salts are very sensitive to impurities caused by oxygen or moisture and only differences between the measured and literature melting temperatures of ±3 K were considered acceptable. For the heat-capacity measurements of the pure compounds, pellets were pressed from the dried salts and filled inside the nickel crucibles to be welded.

The salt mixtures were prepared by directly filling the respective amounts of the individual salts in a container (stainless steel with nickel liner), to avoid a large composition error. This container was hermetically closed and heated for 2 h at a temperature of 100 K higher than the melting temperature of the higher melting pure compound, to ensure complete mixing in the liquid state. After being cooled, the steel container was opened again and the salt mixture inside was milled in a

dx.doi.org/10.1021/ic302168g | Inorg. Chem. 2013, 52, 2404−2411

mortar to a fine powder. With this powder, several pellets were pressed and filled inside the nickel containers, to be closed by laser welding.

After the welding procedure, the weld of every nickel capsule was visually investigated using a microscope to check for small cracks or holes. The total mass of each capsule was measured and compared with the mass before the welding. The crucible was accepted only if the mass difference was within the range of ±0.2 mg. To test the tightness of the crucibles under the conditions of the experiments, they were heated under an argon atmosphere for 5 h at the highest temperature of the respective calorimetric measurements (see Table 3). The masses of the crucibles then were measured again, this time allowing only a maximum mass difference of ±0.1 mg between the masses before and after the heating.

Enthalpy Increment Measurements. The enthalpy increment measurements were done using a multidetector high-temperature calorimeter (Setaram, Type MHTC-96) that was operating in drop mode to derive the high-temperature heat capacities of the $(Li_x\ Na_{1-x})F_x$, $(Li_x\ K_{1-x})F_x$, $(Li_x\ Cs_{1-x})F_x$, and $(Li_x\ Rb_{1-x})F_x$ liquid solutions. In total, 10 samples with different compositions were measured. Tables 1 and 2 list the results of the measurements. The data of the $(Li_x\ Na_{1-x})F_x$ liquid solution (LiF, NaF, and four compositions with x = 0.20, 0.40, 0.60, and 0.80) were taken from our previous publication.[4] Also, the CsF data were taken from an earlier publication by us.[7]

The temperature calibration of the calorimeter was done by measuring several standard calibration metals with defined melting temperatures at the 1990 international temperature scale (ITS-90)[22] at different heating rates (In, Sn, Pb,[23] Zn, Al, Ag, and Au). A more-detailed description of the calibration principle can be found elsewhere,[24] and we refer to that study.

Since drop calorimetry is an isothermal method, the furnace of the calorimeter is heated and stabilized at the dedicated temperature prior to the measurements, to establish a steady value of the heat flow signal (ϕ). Then, a sample, having ambient temperature, is dropped into the sample crucible of the calorimeter. The energy that is necessary to increase the sample temperature to the furnace temperature is withdrawn from the system and the equilibrium is disturbed. During re-establishment of the equilibrium values, ϕ changes, resulting in a peak. This peak has an area that is defined as $\int \phi\, d\tau$, which is proportional to the total enthalpy increment of the sample material. Every 25 min, another sample is dropped into the calorimeter, since experiments have shown that this time is sufficient to restabilize the temperature and heat flow signals.

Drop calorimetry is a relative method; therefore, it is necessary to also measure reference materials with a known heat capacity. With these reference materials, the sensitivity (S_R) of the drop detector is determined in situ. The sensitivity is the measured enthalpy increment (the area of the measured heat flow peak, $\int \phi_R\, d\tau$, of the standard material) divided by the literature value, according to eq 9:

$$S_R = \frac{\int \phi_R\, d\tau}{\int_{T_m}^{T_a} C_{P,R}(T)\, dT} \frac{M_R}{m_R} \tag{9}$$

T_a and T_m are, respectively, the ambient and detector temperatures, with the latter being evaluated as an average from the stable values before and after the drop. The literature value of the standard material is calculated with its mass (m_R), molar mass (M_R), and the temperature function of the molar heat capacity ($C_{P,R}(T)\ dT$). For the measurements, solid sapphire pieces (with masses of 60−120 mg) were used as reference material and the molar heat capacity function was taken from ref 25.

With this sensitivity value S_R, the area of the peak caused by the sample ($\int \phi_S\, d\tau$), and the mass and molar mass of the sample (m_S and M_S, respectively), the molar enthalpy increment of the measured sample (H_m) can be determined according to eq 10, which is the energy needed to heat the sample from ambient temperature (T_a) to the furnace temperature (T_m):

$$\Delta_{T_a}^{T_m} H_m = \frac{\int \phi_S\, d\tau}{S_R} \frac{M_S}{m_S} \tag{10}$$

AUTHOR INFORMATION

Corresponding Author

*E-mail: ondrej.benes@ec.europa.eu.

Notes

The authors declare no competing financial interest.

ACKNOWLEDGMENTS

This work was supported by the EVOL project in the Seventh Framework Programme of the European Commission (Grant Agreement No. 249696). M.B. gratefully acknowledges the support of the European Commission, given in the frame of the program "Training and Mobility of Researchers".

REFERENCES

(1) Beneš, O.; Konings, R. J. M. In *Comprehensive Nuclear Materials*; Konings, R. J. M., Allen, T. R., Stoller, R., Yamanaka, S., Eds.; Elsevier: Oxford, U.K., 2012; Chapter 3.13.

(2) Forsberg, C. W.; Peterson, P. F.; Zhao, H. *J. Solar Energy Eng.* **2007**, *129*, 141−1446.

(3) *Nuclear Hydrogen R&D Plan*; U. S. Department of Energy: Washington, DC, 2004.

(4) Beneš, O.; Konings, R. J. M.; Künzel, C.; Sierig, M.; Dockendorf, A.; Vlahovic, L. *J. Chem. Thermodyn.* **2009**, *41*, 899−903.

(5) Desai, P. D. *Int. J. Thermophys.* **1987**, *8*, 763−780.

(6) Chase, M. W. *NIST—JANAF Thermochemical Tables*, 4th Edition; Journal of Physical and Chemical Reference Data Monograph 9; National Institute of Standards and Technology (NIST): Gaithersburg, MD, 1998.

(7) Beneš, O.; Konings, R. J. M.; Sedmidubský, D.; Beilmann, M.; Valu, O. S.; Capelli, E.; Salanne, M.; Nichenko, S. *J. Chem. Thermodyn.* **2013**, *57*, 92−100.

(8) Rollet, A.-L.; Salanne, M. *Annu. Rep. Prog. Chem., Sect. C.* **2011**, *107*, 88−123.

(9) Baranyai, A.; Ruff, I.; McGreevy, R. L. *J. Phys. C: Solid State Phys.* **1986**, *19*, 453−465.

(10) Dracopoulos, V.; Papatheodorou, G. N. *Phys. Chem. Chem. Phys.* **2000**, *2*, 2021−2025.

(11) Salanne, M.; Vuilleumier, R.; Madden, P. A.; Simon, C.; Turq, P.; Guillot, B. *J. Phys.: Condens. Matter* **2008**, *20*, 494207-1−494207-8.

(12) Dedyukhin, A. E.; Apisarov, A. P.; Redkin, A. A.; Tkacheva, O. Y.; Zaikov, Y. P. *Light Metals* **2008**, *TMS (2008)*, 509−511.

(13) Holm, J. L.; Kleppa, O. J. *J. Chem. Phys.* **1968**, *49*, 2425−2430.

(14) Khokhlov, V.; Ignatiev, V.; Afonichkin, V. *J. Fluorine Chem.* **2009**, *130*, 30−37.

(15) Janz, G. J. *J. Phys. Chem. Ref. Data* **1988**, *17* (Suppl. 2), 1−309.

(16) Macleod, A. C.; Cleland, J. *J. Chem. Thermodyn.* **1975**, *7*, 103−118.

(17) Ribeiro, M. C. C. *J. Phys. Chem. B* **2003**, *107*, 4392−4402.

(18) Holm, J. L. *Acta Chem. Scand.* **1971**, *25*, 3609−3615.

(19) Cohen, S. I.; Powers, W. D.; Greene, N. D. *A Physical Property Summary for ANP Fluoride Mixtures*, AEC Research and Development Report ORNL-2150, C-84, M-3679; Oak Ridge National Laboratory (ORNL): Oak Ridge, TN, USA, 1956.

(20) Shannon, R. D. *Acta Crystallogr., Sect. A: Cryst. Phys., Diffr., Theor. Gen. Crystallogr.* **1976**, *A32*, 751−767.

(21) Beilmann, M.; Beneš, O.; Konings, R. J. M.; Fanghänel, T. *J. Chem. Thermodyn.* **2011**, *43*, 1515−1524.

(22) Preston-Thomas, H. *Metrologia* **1990**, *27*, 3−10.

(23) Bedford, R. E.; Bonnier, G.; Maas, H.; Pavese, F. *Metrologia* **1996**, *33*, 133−154.

(24) Beneš, O. *Thermodynamics of Molten Salts for Nuclear Applications*, Ph.D. Thesis, ICT Prague, Prague, Czech Republic, 2008.

(25) Standard Reference Material No. 720; National Institutes of Standards and Technology (NIST): Gaithersburg, MD.